Solar Energy 201 (2020) 461–468

Contents lists available at ScienceDirect

Solar Energy

journal homepage: www.elsevier.com/locate/solener

Regulation of surface texturization through copper-assisted chemical etching for silicon solar cells

Yan Zhao, Yaoping Liu*, Wei Chen, Juntao Wu, Quansheng Chen, Hanbo Tang, Yan Wang, Xiaolong Du*

Songshan Lake Materials Laboratory, Dongguan, Guangdong 523808, China
Key Laboratory for Renewable Energy, Beijing Key Laboratory for New Energy Materials and Devices, Beijing National Laboratory for Condensed Matter Physics, Institute of Physics, Chinese Academy of Sciences, Beijing 100190, China
School of Physical Sciences, University of Chinese Academy of Sciences, Beijing 100049, China

ARTICLE INFO

Keywords:
Silicon texturization
Copper nanoparticles
Surface morphology
Metal-assisted chemical etching

ABSTRACT

Various structures were fabricated through a copper-assisted chemical etching method for texturization of monocrystalline silicon solar cells, including nanopore, inverted pyramid, V-groove, upright pyramid and hybrid structures. Structural characteristics, etching processes and anti-reflection abilities of the textured structures were systematically analyzed. Brand new texturization results were observed in this research. A possibility that the copper-catalyzed textured structures can be terminated with silicon {1 1 0} crystalline planes is proposed, and the evidence is provided. Furthermore, the transformation of the textured structures was studied, and the agglomerated behavior of the copper nanoparticles deposited on the silicon surface during etching was demonstrated to be a prominent source for the formation of various textured structures. The influences of etchant components and initial silicon surface states on the agglomeration were also studied. Consequently, the surface morphology and anti-reflection property of the textured silicon wafers can be well regulated by controlling the agglomeration of deposited copper nanoparticles in the etching process. A minimum average reflectance of 6.19% in the wavelength range of 300–1000 nm was obtained, which indicates great potentials of this copper-assisted texturization process for the photovoltaic application. In addition, according to the experimental results and analyses, a practical guidance for texturization of silicon solar cells is provided.

1. Introduction

Texturization is an essential step in the manufacturing process for silicon (Si) solar cells, as conversion efficiencies of the solar cells can be significantly improved with an increased light absorption from Si wafers (Baker-Finch and McIntosh, 2011; Basher et al., 2018a; Basher et al., 2019a; Campbell and Green, 1987). As a result, a wide variety of texturization methods have been proposed.

Anisotropic etching in alkaline solutions is the most commonly used texturing method for mono-crystalline Si (c-Si) solar cells, and its excellent light trapping ability in random pyramid structure fabricated through alkaline etching has been verified in previous studies (Baker-Finch and McIntosh, 2011; Basher et al., 2018b; Basher et al., 2019a,b,c; Biswas et al., 2019; Vazsonyi et al., 1999). Unfortunately, due to its remarkable anisotropic etching characteristic, alkaline etching cannot be applied for the texturization of multi-crystalline silicon (mc-Si) wafers considering the different crystallographic orientations between the grains on mc-Si wafers. Therefore, isotropic etching processes should be utilized for texturization when mc-Si solar cells are fabricated. Nevertheless, with the popularization of the diamond wire sawn (DWS) technique, the traditional acid texturing process has lost its application value in the photovoltaic industry; it is difficult to completely remove the damaged layers on a DWS mc-Si surface (Bidiville et al., 2009; Chen et al., 2014; Zhuang et al., 2016). Instead, a metal-assisted chemical etching (MACE) process has been widely used when fabricating mc-Si solar cells (Chen et al., 2019; Yang et al., 2019; Zhuang et al., 2016). In industry, the Ag-assisted chemical etching method combined with an alkaline pre-treatment as well as an acid post-treatment has become the mainstream. However, this complex and high-cost texturing process is not suitable for the texturization of c-Si wafers because the nanostructures obtained through the Ag-catalyzed etching process will lead to severe carrier recombination, subsequently decreasing conversion efficiencies. On the other hand, in addition to the above-mentioned wet etching methods, reactive ion

* Corresponding authors.
E-mail addresses: ypliu@iphy.ac.cn (Y. Liu), xldu@iphy.ac.cn (X. Du).

https://doi.org/10.1016/j.solener.2020.03.013
Received 6 January 2020; Received in revised form 18 February 2020; Accepted 4 March 2020

etching (RIE) (Garnett and Yang, 2010; Sai et al., 2006), solid-liquid-vapor growth (Kayes et al., 2007; Kelzenberg et al., 2010) and laser modification (Her et al., 1998; Nayak et al., 2011) methods are also frequently used texturing techniques, but the industrial applications of these methods have been limited because of the high facility costs and low productivities.

Previous studies have shown that the one-step Cu-assisted chemical etching (Cu-ACE) process can be utilized to fabricate micron-scale random inverted pyramid structure on c-Si wafers due to its outstanding anisotropic etching characteristic (Wang et al., 2017, 2015). Moreover, the excellent light-trapping properties of the textured inverted pyramid structure have been revealed. The average reflectance can be dramatically reduced to less than 5% for inverted pyramid textured c-Si wafers, showing great advantages over the random pyramid structure prepared through the alkaline etching (Wang et al., 2017, 2015; Yang et al., 2017). In addition, various nanostructures have also been acquired through the Cu-ACE process, including nanowire (Huang et al., 2010), nanopore (M. K. Basher et al., 2019b; Cao et al., 2015; Lee et al., 2011; Lu and Barron, 2014; Zheng et al., 2014) and crater (Cao et al., 2015; Zheng et al., 2014) structures, indicating that the cheaper Cu can be used as a substitute for the expensive Au or Ag in the MACE process for the texturization of mc-Si wafers. Therefore, the Cu-ACE method can be utilized as a universal texturization technique for all kinds of Si wafers to fabricate structures with micro or nano sizes. More importantly, the Cu-ACE process has shown many distinct advantages in texturization, including excellent cell performances, lower texturization costs and versatile facilities for mass production of both c-Si and mc-Si solar cells. Consequently, it exhibits great potential for effective texturization management in the photovoltaic industry.

In this study, a systematic investigation was performed to study the etching process and reaction mechanism of the Cu-ACE method. In the experiments, anisotropic etching results different from previous studies have been observed, and we speculated that the textured structure of the Cu-ACE might be terminated with other crystalline planes except for the {1 1 1} crystalline plane. Transformation between different textured structures was proposed, and the agglomerated behavior of the deposited Cu-nanoparticles (Cu-NPs) on the surface of Si wafer was proved to be the prominent factor for the texturization results. Furthermore, the impacts resulted from the experimental conditions and surface states of the DWS c-Si wafers in the etching process were discussed; thus, effective texturization regulation for silicon solar cells was achieved. Superior anti-reflection performances of the textured structures were exhibited in this research. Based on the experimental results and analyses, a practical guidance for the Cu-ACE method to be applied in actual applications was presented in this research.

2. Experimental section

(1 0 0)-Oriented DWS monocrystalline Si wafers (p-type boron-doped, 200±10 μm thick, resistance 1–3 Ω·cm) were used in this study. Before etching, the DWS c-Si wafers were cut into small pieces, with dimensions of 30 mm × 30 mm, for texturization. These raw c-Si samples were immersed in acetone, ethanol and deionized water successively for ultrasonic cleaning and then blow-dried with N_2 gas. The cleaned samples were then textured in a mixed solution containing $Cu(NO_3)_2$, HF and H_2O_2 to obtain different surface structures. Table 1 summarizes the concentrations of the components $Cu(NO_3)_2$, HF and H_2O_2 in the etchant solutions for different textured structures, while the etching times and temperatures are listed as well. After etching, the samples were immediately immersed in deionized water to wash off the residual solution on the surface of the samples. To remove the deposited Cu-NPs on the surface of the etched samples, the samples were immersed in an aqueous HNO_3 solution for 20 min and dried with blowing N_2 gas.

In addition, HF treatment was adopted to remove the amorphous-Si (a-Si) layer on the DWS c-Si surface in this research. To obtain the HF-treated samples, the cleaned DWS c-Si samples were immersed in a 10% aqueous HF solution for 6 h at room temperature.

Scanning electron microscopy (SEM, Zeiss Sigma 300) was utilized to investigate the surface morphologies of the textured samples. A UV–Vis-NIR spectrophotometer (Agilent Cary 7000) with an integrating sphere was employed to measure the reflectance spectra of the samples in a wavelength range of 300 nm–1000 nm. Raman spectra of the raw DWS c-Si and HF-treated samples were acquired using laser confocal micro-Raman spectroscopy (Horiba LabRAM HR Evolution). The excitation wavelength of the laser was 532 nm, and the diameter of the laser spot was approximately 1 μm.

3. Results and discussion

Our previous studies have revealed that the Cu-ACE method can be utilized to fabricate various surface structures on Si substrates (Wang et al., 2017, 2015). Fig. 1 illustrates the different textured structures we fabricated through this Cu-induced etching method, including the nanopore, inverted pyramid, V-groove and upright pyramid structure. The corresponding experimental conditions are listed in Table 1. The concentration of $Cu(NO_3)_2$ in the etchant solution for nanopore texturization was much lower when compared with that of other etchants. Previous studies have shown that the formation of a small-sized nanopore structure was mainly due to the relatively low concentrations of Cu^{2+} in the etching solutions since the size of the deposited Cu-NPs on the substrates would be quite small under such conditions and the size of the structures would be limited by the tiny Cu-NPs (Cao et al., 2015; Lu and Barron, 2014).

As for the microstructures we obtained in the experiments, the most important difference between the experimental conditions for these textured structures was the component concentration. The concentration of H_2O_2 is shown to be a major impact factor for morphology control in this electrochemical etching process (Cao et al., 2015; Li et al., 2017; Lu and Barron, 2014; S. Zhao et al., 2019). In this research, we summarized the experimental conditions of the aforementioned three micron-sized textured structures and found that both the concentrations of HF and H_2O_2 had significant impacts on the formation of different structures.

The relationships between the different textured surface structures and the experimental conditions are described in Fig. 2a. The Cu^{2+} concentration in the etchant was kept at 0.1 M in these experiments, while the samples were all etched at 30 °C for 300 s. The evolution of the surface morphologies can be clearly seen in Fig. 2a, and three cases of etching can be identified according to the textured structures. When the concentration of HF was 4.75 M, the upright pyramid structure was obtained through the Cu-ACE process as the H_2O_2 concentration in the

Table 1
Summary of etching conditions for Cu-ACE.

$c(Cu^{2+})$/mol L^{-1}	c(HF)/mol L^{-1}	$c(H_2O_2)$/mol L^{-1}	T/°C	t/s	Structure
0.005	4.50	0.90	30	300	Nanopore
0.10	4.50	0.90	30	300	Upright pyramid
0.10	4.50	1.20	30	300	V-groove
0.10	4.50	1.50	30	300	Inverted pyramid

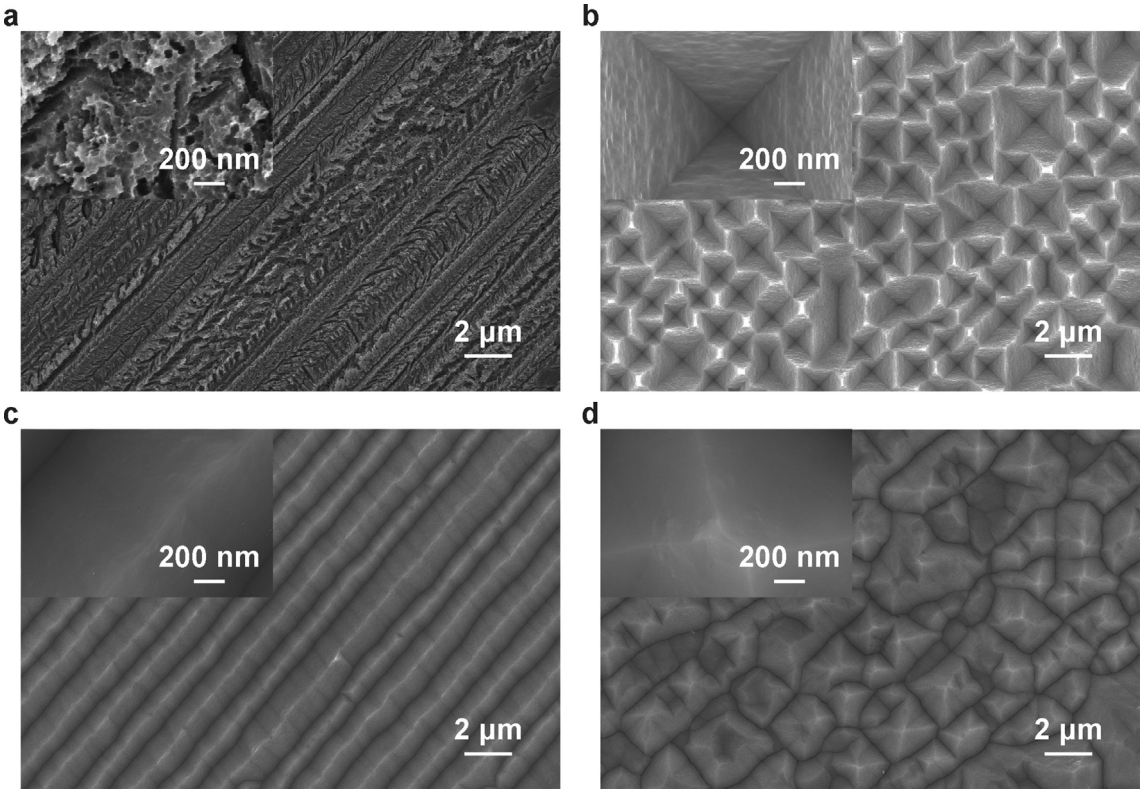

Fig. 1. SEM images of different textured structures on DWS c-Si wafers fabricated through the Cu-ACE process: nanopore (a), inverted pyramid (b), V-groove (c) and upright pyramid (d).

etching solution was low. When the H_2O_2 concentration increased to 1.20 M, the surface structure gradually converted from the upright pyramid into a hybrid structure, which consisted of upright pyramids and V-shaped grooves (see Fig. 2b). In addition, the experimental results showed that a universal V-groove structure could be fabricated with certain concentrations of HF and H_2O_2 in the solution. As the H_2O_2 concentration was further increased, inverted pyramids began to form on the substrates, and its proportion gradually increased. Accordingly, the proportion of the V-groove structure was decreased. Fig. 2c represents the SEM image of the hybrid structure consisting of V-grooves and inverted pyramids, which was fabricated when the HF and H_2O_2 concentrations were 4.75 M and 1.50 M, respectively. Furthermore, when the concentration of H_2O_2 in the etchant was sufficiently high, the surface of the c-Si samples was overlaid by randomly distributed inverted pyramids. As shown in Fig. 2a, the boundaries of the adjacent regions representing the different texturization cases are approximately straight, indicating that the critical concentrations of H_2O_2 and HF had approximately linear relationships when the structural transformations occurred. Based on these experimental results and analyses, better morphology control can be achieved when fabricating the above-mentioned micron-sized surface structures through the Cu-ACE method.

The experimental results of the Cu-catalyzed anisotropic etching we observed in our research were slightly different from previous studies. Numerous studies have confirmed that significant anisotropy can be exhibited in the Cu-ACE process; hence, it has been regarded as one of the conventional preparation methods for inverted pyramid structure

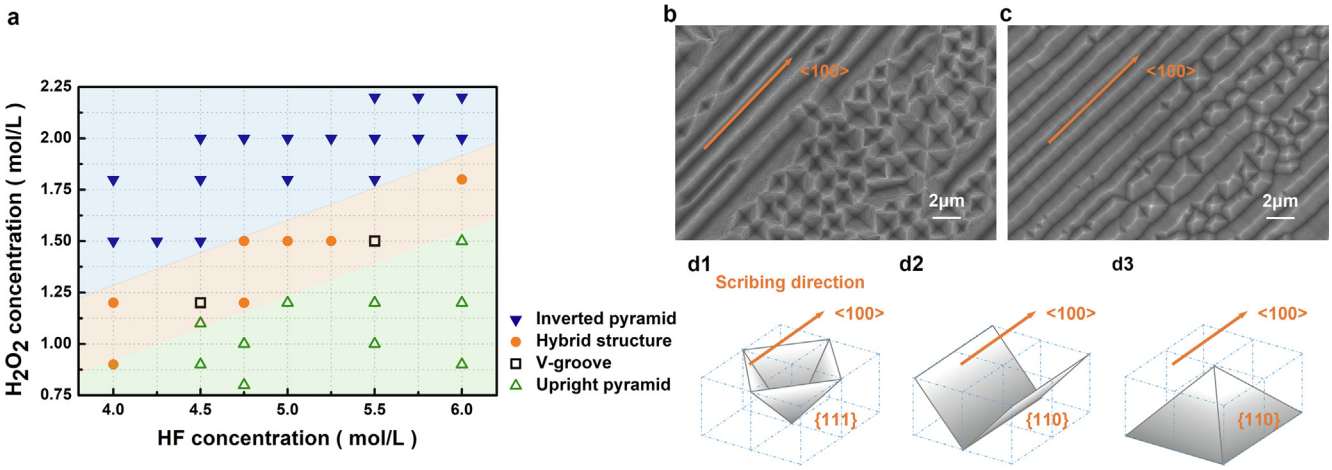

Fig. 2. The evolution of textured morphologies in the Cu-ACE process (a). SEM images of the hybrid structure consisting of inverted pyramids and V-grooves (b), and the hybrid structure consisting of V-grooves and upright pyramids (c). Schematic diagrams of the inverted pyramid, V-shaped groove and upright pyramid (d1-d3). The arrows represent the wafer slicing directions on the samples.

(Li et al., 2017; Wang et al., 2017, 2015; Wu et al., 2018; Yang et al., 2017, p. 87; S. Zhao et al., 2019). For the inverted pyramid structure, the sidewalls are usually terminated with Si {1 1 1} crystalline planes, and the angle between the sidewall and a {1 0 0} crystalline plane is 54.7°. This anisotropic etching phenomenon has been proven to mainly result from the different surface bond densities of the crystalline planes. Therefore, the Cu^{2+} ions in the etchant are more likely to capture electrons from the {1 0 0} crystalline planes than the {1 1 1} planes while etching, resulting in higher probabilities for Cu-NPs to nucleate on the Si {1 0 0} planes. As a result, the Cu-NPs deposited on the {1 0 0} crystalline planes usually have large sizes and high densities, thus resulting in a higher etching rate. Due to the differences in etching rate, the etched structures are generally composed of {1 1 1} crystal planes (Wang et al., 2017, 2015). Consistent with the previous experimental results, the inverted pyramid structures, where the sidewalls were terminated with the {1 1 1} crystalline planes on Si substrates, were also fabricated in our experiments. Nevertheless, it is worth noting that the V-groove structure and upright pyramid structure we prepared using the Cu-ACE method were not terminated with the Si {1 1 1} planes in Fig. 2b and 2c. Our recent research has revealed that the V-shaped grooves prepared using the Cu-ACE method on the c-Si wafers were parallel to the diamond wire slicing direction, i.e., the ⟨1 0 0⟩ crystal orientation for the c-Si wafers, and the sidewalls of the grooves were terminated with {1 1 0} crystalline planes (Y. Zhao et al., 2019). Therefore, considering the relative positions of the grooves and upright pyramids in the hybrid structure, shown in Fig. 2c, it can be inferred that the upright pyramids we obtained on the c-Si substrates were consisted of the Si {1 1 0} planes. The schematic diagrams of the inverted pyramid, V-shaped groove and upright pyramid fabricated in this research are shown in Fig. 2d1-d3.

To further verify the conclusions, the same etching experiments were conducted on c-Si wafers in which the slicing directions were all parallel to the ⟨1 1 0⟩ orientation. The surface morphology of the inverted pyramid and V-groove hybrid structure is shown in Fig. 3a, while Fig. 3b exhibits the hybrid structure of upright pyramids and V-grooves. The V-shaped grooves in these two hybrid structures were parallel to the Si ⟨1 1 0⟩ orientation, and the sidewalls were terminated with {1 1 1} crystalline planes. According to the relative positional relationships between the V-grooves, inverted pyramids and upright pyramids in the hybrid structures, it can be speculated that the inverted pyramids were still composed of the {1 1 1} planes, while in this case, the upright pyramids were terminated with the {1 1 0} crystalline planes. Schematic diagrams are shown in Fig. 3c1-c3. As a consequence, except for the common exposure of {1 1 1} planes, our experimental results also showed a possibility for the {1 1 0} crystalline planes to be exposed after the Cu-assisted anisotropic etching process.

To regulate the Cu-assisted texturization process more effectively, the impacts of initial Si surface features on etching in the Cu-ACE process were considered. Numerous studies have been conducted to investigate the etching performances when the DWS Si wafers were used as substrates in wet acidic texturing and alkaline texturing processes (Bidiville et al., 2009; Chen et al., 2015, 2014; Lippold et al., 2014; Meinel et al., 2012; Zhuang et al., 2016). Previous studies have demonstrated that phase transformation would occur during the wafer slicing for DWS Si wafers, and a-Si and meta-stable phases, including Si-III and Si-VII phases, could be formed in the smooth groove region on the surface due to the stress release while slicing (Bidiville et al., 2009; Domnich and Gogotsi, 2002; Gassilloud et al., 2005; Hu et al., 1986). It is generally believed that a-Si will exhibit lower etching rates owing to lower dangling bond densities and lower back bond energy levels compared with those of the atoms on the Si {1 0 0} surface (Biegelsen and Stutzmann, 1986). Thus, the a-Si can act as a mask on the Si wafer surface in the texturization step, resulting in the structural inhomogeneity of the textured Si wafers (Bidiville et al., 2009; Chen et al., 2015, 2014; Meinel et al., 2012).

In this research, experiments were performed to further investigate

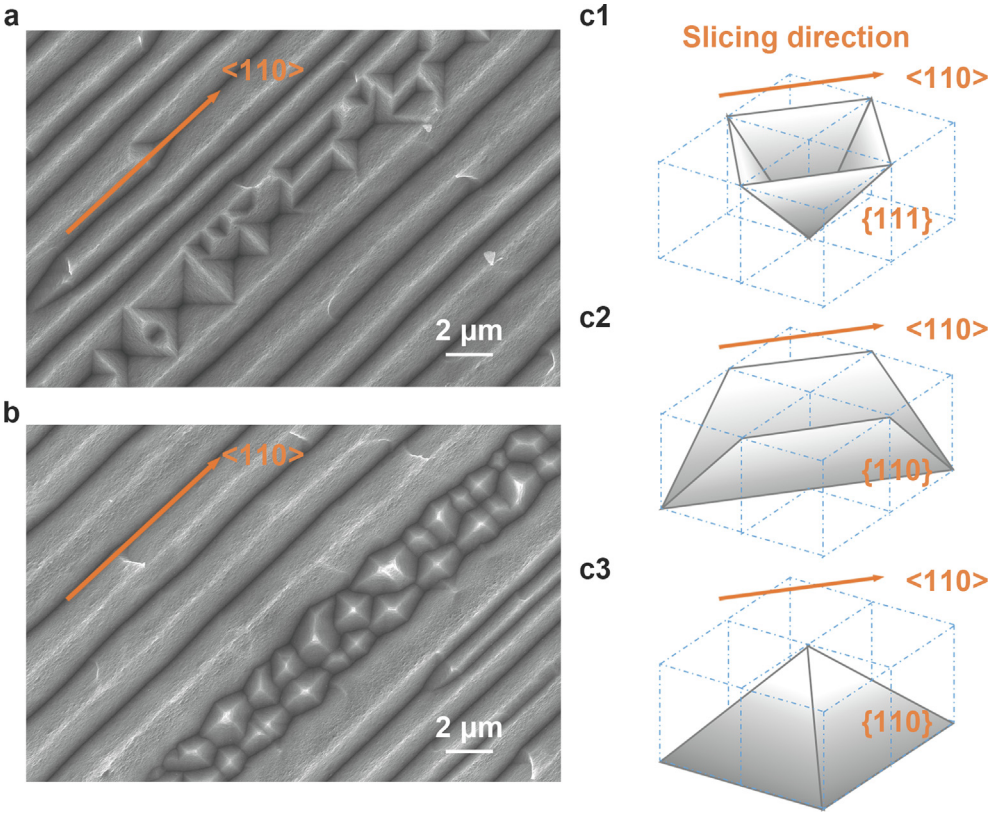

Fig. 3. SEM images of the hybrid structure consisting of inverted pyramids and V-grooves (a), and the hybrid structure consisting of V-grooves and upright pyramids (b). Schematic diagrams of the inverted pyramid, V-shaped groove and upright pyramid (c1-c3). The arrows represent the wafer slicing directions on the samples.

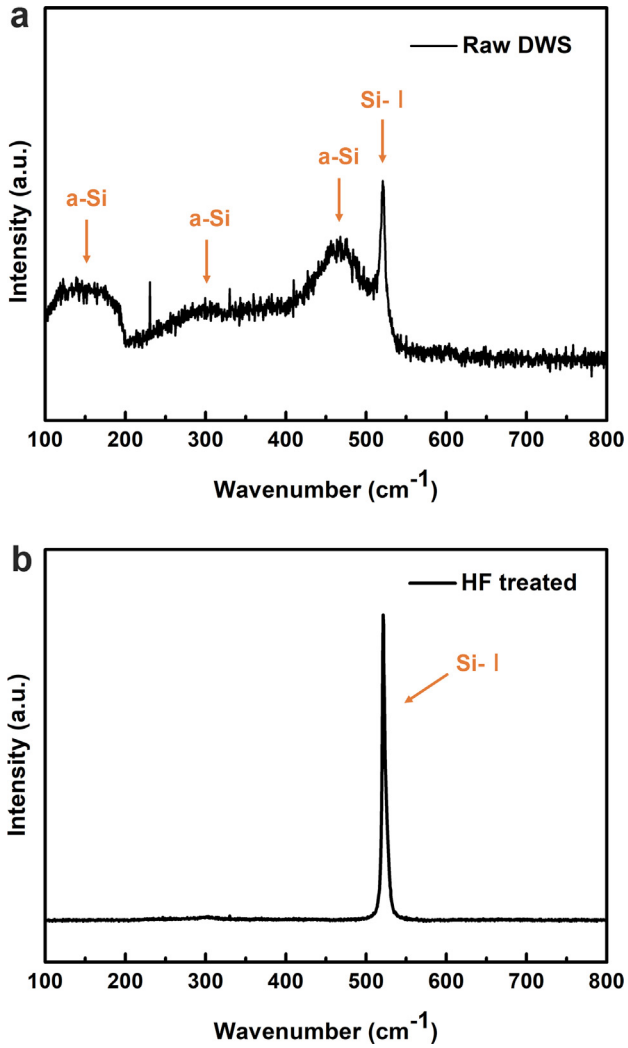

Fig. 4. Raman spectra of the raw DWS c-Si sample (a) and the HF-treated sample (b).

the a-Si on the DWS c-Si wafers and its influences on the Cu-ACE process. For comparison, DWS c-Si samples with and without an a-Si layer on the surface were employed. In our experiments, the DWS c-Si samples were immersed in an aqueous HF solution for 6 h to completely remove the a-Si layer on the Si surface. The Raman spectra of the raw DWS c-Si sample and the HF-treated sample are provided in Fig. 4a and b. It should be noted that the a-Si distributed unevenly on the surface of DWS c-Si wafers, and hence, the Raman analyses were both conducted on the smooth region for these two samples. For the raw DWS c-Si sample, except for the sharp peak at the wavenumber of 520 cm^{-1} that represented the pristine Si-I, broad peaks could be distinguished at approximately 150 cm^{-1}, 300 cm^{-1} and 470 cm^{-1} in Fig. 4a, indicating the existence of the a-Si phase. For the HF-treated sample, see Fig. 4b, only one significant peak representing pristine Si-I can be found at 520 cm^{-1}, which meant that the a-Si on the sample was completely etched away after the HF treatment.

The HF-treated DWS c-Si samples and the raw DWS c-Si samples were then employed in the Cu-ACE process. The etching performances as well as the textured surface morphologies were compared and analyzed to examine the impact of the a-Si layer formed during wafer slicing (see Fig. 5). The concentrations of Cu^{2+}, HF and H_2O_2 are 0.10 M, 5.50 M and 1.50 M in the etchant solution, respectively, while the etching temperature was 30 °C. As shown in Fig. 5, the HF-treated samples possessed higher Cu-NP densities when compared with the raw DWS c-Si samples under the same etching time. V-shaped grooves that were parallel to the wafer slicing direction were formed on both types of samples, and few obvious differences were found between the textured V-groove structures. It can be inferred that the a-Si on the surface of DWS c-Si wafers would hinder the deposition of the Cu-NPs, thus leading to a lower density of the metal particles, which was in accordance with previous studies. Nevertheless, the a-Si on the surface of DWS wafers was not the most important cause for the formation of V-grooves.

The Cu-NPs deposited on the Si surface exhibited approximately line-shaped distributions from beginning to end during the V-groove etching, and the lines were all parallel along the wafer slicing directions, as illustrated in Fig. 5. This deposition phenomenon differed from the inverted pyramid texturization, as it showed an obvious tendency for the Cu-NPs to be deposit discretely in random dots when the inverted pyramid textured Si was fabricated. Based on the experimental phenomena, the formation of the V-shaped grooves was speculated to be closely related to the distinct linear Cu-NPs agglomeration on the surface of the samples. To better regulate the texturization, the formation reasons for the line-shaped Cu-NPs agglomeration should be studied. At the initial etching stage, the Cu-NPs had already selectively deposited on the Si surface when etched for 5 s, see Fig. 5a2 and b2. Microcracks along the slicing direction were observed, and the nanoparticles were mainly nucleated near the cracks; meanwhile, few were deposited on the flat areas, as it was easier for Cu^{2+} to capture electrons

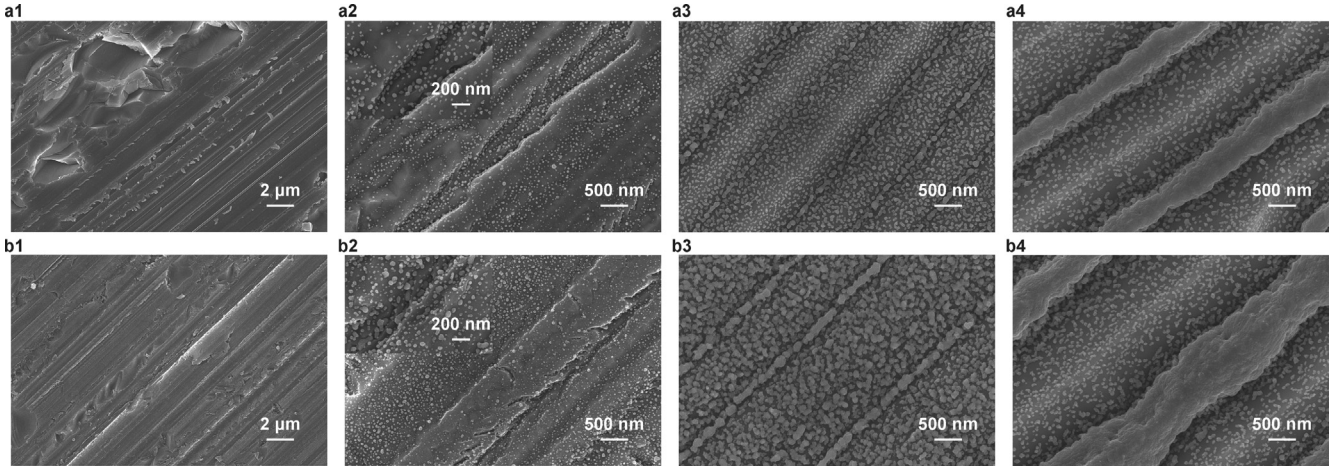

Fig. 5. SEM images of V-groove etching processes on raw DWS c-Si wafers for 0 s (a1), 5 s (a2), 60 s (a3) and 180 s (a4). SEM images of V-groove etching processes on HF-treated DWS c-Si wafers for 0 s (b1), 5 s (b2), 60 s (b3) and 180 s (b4).

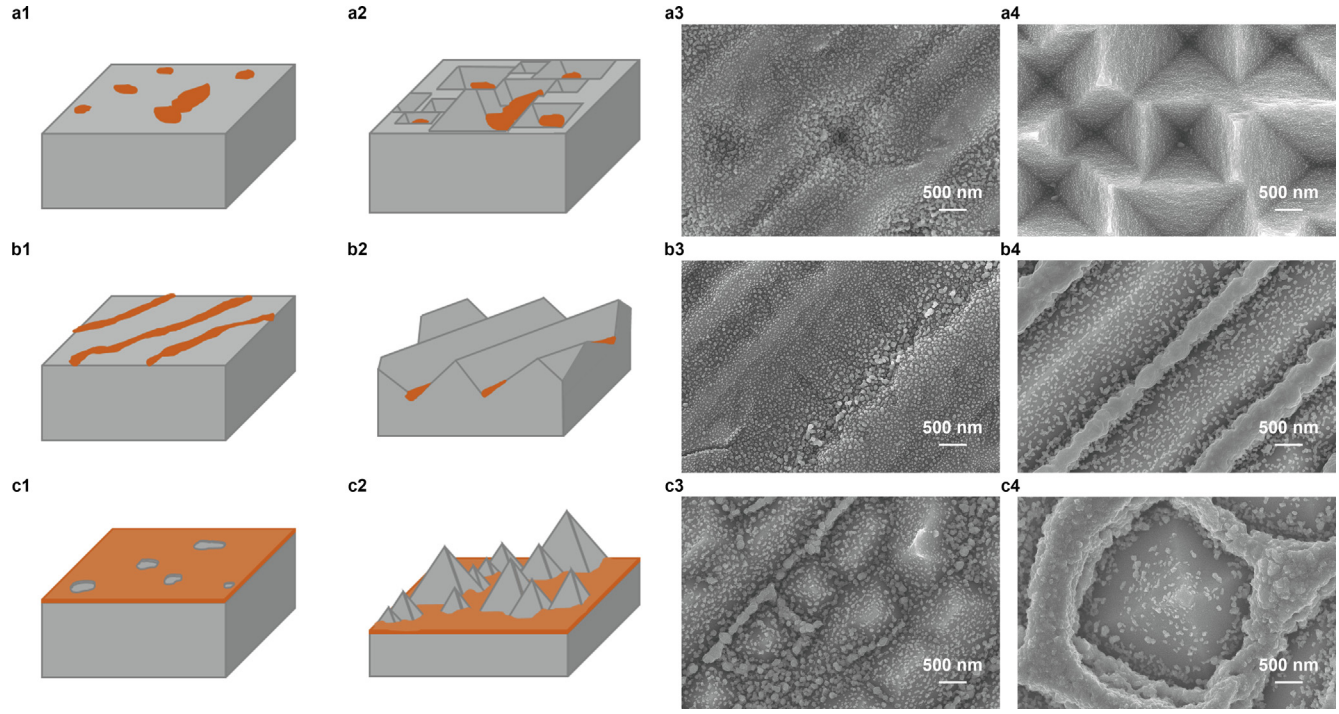

Fig. 6. Formation processes of inverted pyramid, V-groove and upright pyramid structures. Schematic diagrams for the formation of the inverted pyramid structure at the initial stage (a1) and end stage (a2). SEM images for the formation of the inverted pyramid structure after 10 s (a3) and 180 s (a4). Schematic diagrams for the formation of the V-groove structure at the initial stage (b1) and end stage (b2). SEM images for the formation of the V-groove structure after 10 s (b3) and 180 s (b4). Schematic diagrams for the formation of the upright pyramid structure at the initial stage (c1) and end stage (c2). SEM images for the formation of the upright pyramid structure after 10 s (c3) and 180 s (c4).

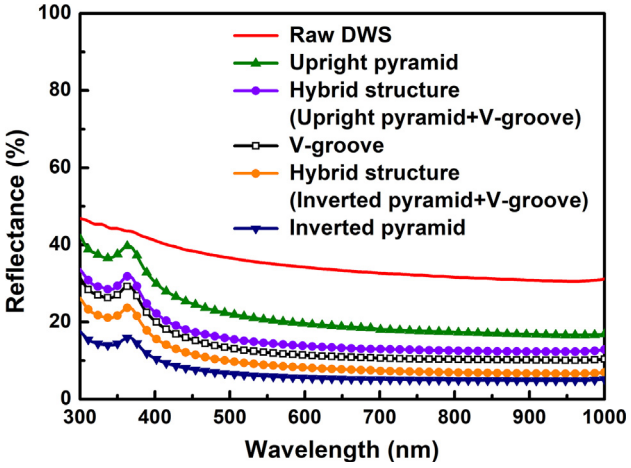

Fig. 7. Reflectance spectra of the raw DWS c-Si wafer and different textured samples fabricated through the Cu-ACE method.

and then nucleate on the regions where defects were densely distributed because the Si-Si bonds were weaker in these regions (Jenkins, 1977; Kulkarni et al., 2002; Wang et al., 2017). Relevant studies have revealed that the through cracks with wafer length were formed after scratching for the DWS Si wafers (Bidiville et al., 2010; Gassilloud et al., 2005). Therefore, we speculate that the tendency for the Cu-NPs to be deposited along the slicing direction probably results from the through cracks on the DWS wafer surface. In the subsequent reaction processes, the sizes and the densities of the Cu-NPs increased with the reaction time. Eventually, the samples were covered by the line-shaped agglomerated Cu-NPs, while some discrete particles were distributed between the lines, and grooves were formed. In addition, since the a-Si distributed on the smooth and flat regions could result in a lower etching rate, the difference in etching rate was intensified, and the formation of the Si V-groove structure was accelerated. Therefore, the agglomerated behavior of the Cu-NPs can be regarded as an important factor for the formation of the V-groove structure.

Moreover, the experimental results revealed that the component concentrations in the etching solutions, especially the concentrations of HF and H_2O_2, can also significantly affect the formation of textured structures. To verify the impacts caused by the changes in HF and H_2O_2 concentrations in texturing, further investigations were conducted. For the Cu-ACE, the reactions that occurred during the etching process are as follows (Wang et al., 2017, 2015):

Cathode reaction:

$$Cu^{2+} + 2e^- \rightarrow Cu(s) \quad (1)$$

$$H_2O_2 + 2H^+ \rightarrow 2H_2O + 2h^+ \quad (2)$$

Anode reaction:

$$Si(s) + 2H_2O \rightarrow SiO_2 + 4H^+ + 4e^- \quad (3)$$

$$SiO_2(s) + 6HF \rightarrow H_2SiF_6 + 2H_2O \quad (4)$$

Table 2
Average reflectances of different textured samples in the wavelength range of 300–1000 nm.

Structure	Inverted pyramid	Hybrid structure (Inverted pyramid + V-groove)	V-groove	Hybrid structure (Upright pyramid + V-groove)	Upright pyramid	Raw DWS
Average reflectance/%	6.19	9.02	12.47	14.79	20.51	34.43

During the etching reaction, the H_2O_2 and Cu^{2+} can simultaneously inject holes into the Si to form SiO_2 on the sample surface. In addition, since the redox potential of H_2O_2/H_2O is higher than that of Cu^{2+}/Cu, the deposited Cu-NPs can be oxidized into Cu^{2+} ions with holes injected from H_2O_2. The reaction can be described as (Wang et al., 2017):

$$Cu + H_2O_2 + 2H^+ \rightarrow 2H_2O + Cu^{2+} \quad (5)$$

Therefore, the H_2O_2 concentration in the etchant will dramatically influence the Cu-NPs deposition and agglomeration on the surface of Si wafers.

According to our experimental results shown in Fig. 2a, as the HF concentration remained constant, the textured surface structure gradually changed from the inverted pyramid structure to the V-groove structure and finally turned into the upright pyramid structure with the decrease of H_2O_2 concentration in the etchant solution. This transformation of the textured structures was probably resulted from the variation in the agglomerated behavior of deposited Cu-NPs on the samples. Fig. 6 illustrates the formation processes and mechanisms of different textured structures. While etching, when the H_2O_2 in the etchant solution was sufficient, the deposited Cu-NPs on the Si surface would be easily oxidized into the Cu^{2+} ions by H_2O_2. Therefore, the density of the deposited Cu-NPs was relatively low, and most of the particles were distributed discretely on the Si surface, as shown in Fig. 6a1 and a3. Our previous research has revealed that the formation of the inverted pyramid structure was resulted from the combined effects of anisotropic etching and a localized reaction process, while the upright pyramid structure was fabricated when the anisotropic etching was taking place almost everywhere on the whole surface of the samples (Chen et al., 2018). Therefore, this localized anisotropic etching process finally led to the formation of the inverted pyramid structure, see Fig. 6a2 and a4. Additionally, the formation process of the nanostructures was similar to this case, but the size of the Cu-NPs was greatly limited because of the low concentration of Cu^{2+} ions. A higher Cu-NPs deposition rate was observed when the H_2O_2 concentration was reduced, so the density of the deposited Cu-NPs was increased. The agglomeration degree of the Cu-NPs tended to increase. Under this circumstance, the surface characteristics of raw DWS c-Si wafers became the prominent influencing factor in the etching process. Based on the analyses presented above, the Cu-NPs preferentially nucleated in lines parallel to the wafer slicing direction on the Si surface, and thus, the line-shaped Cu-NPs on the entire surface were obtained. The V-shaped grooves arranged in parallel were eventually formed, as shown in Fig. 6b1-b4. As the H_2O_2 concentration in the etchant was further lowered, the oxidation of Si primarily relied on hole injections from Cu^{2+} ions. Meanwhile, the Cu-NPs were hard to be oxidized due to the insufficient H_2O_2 concentration. The density of the Cu-NPs deposited on the Si surface was notably increased, and the agglomerated Cu-NPs can be approximated as a planar distribution. At this point, an upright pyramid structure was fabricated under this whole anisotropic surface etching process, as shown in Fig. 6c1-c4. As a consequence, the Cu-ACE process can be greatly influenced by the agglomerated behavior of the deposited Cu-NPs on Si wafers, which provides a possibility for the regulation of texturization.

The anti-reflection properties of the samples with different textured structures have been investigated. The reflectance spectra of the samples in the wavelength range of 300–1000 nm are provided in Fig. 7, and the average reflectances are listed in Table 2. As shown in Fig. 7, the inverted pyramid structure showed the lowest average reflectance of 6.19%, while the V-groove textured c-Si sample exhibited a higher but still acceptable anti-reflection performance. However, the upright pyramid structure showed no obvious advantage in light absorption because of the relatively high average reflectance, which exceeded 20%. The anti-reflection performances of the hybrid structured samples were also tested, see Fig. 7, and the reflectance of the hybrid structure tended to be in between the reflectance values of the two particular structures in the hybrid. The above performances and results demonstrated the effective control of the anti-reflection performance through the Cu-assisted texturization.

4. Conclusions

Various surface structures have been fabricated on DWS c-Si substrates through Cu-ACE processes. A possibility that the structures terminated with Si {1 1 0} crystalline planes can also be fabricated using this Cu-assisted anisotropic etching method was proposed. Transformation between different textured structures was discussed. The agglomerated behavior of the deposited Cu-NPs, which was greatly influenced by the concentrations of HF and H_2O_2 in etchant solution, was proved to be a prominent factor for the texturization. According to the experimental results, the surface morphology would transform from the inverted pyramid to the V-groove and finally to the upright pyramid with the increasing deposition density and agglomeration degree of the Cu-NPs. In addition, the a-Si layer on DWS c-Si wafers was proved to hinder the deposition of the Cu-NPs, thus leading to a lower etching rate in Cu-ACE. Different anti-reflection performances were exhibited, and a minimum average reflectance of 6.19% was obtained in the wavelength range of 300–1000 nm. In summary, the texturization process and anti-reflection performance of the Si solar cells can be effectively regulated by controlling the agglomerated behavior of Cu-NPs in the Cu-catalyzed anisotropic etching process, indicating great potential for the Cu-ACE method to be widely applied in the photovoltaic field.

Declaration of Competing Interest

The authors declare that they have no known competing financial interests or personal relationships that could have appeared to influence the work reported in this paper.

Acknowledgements

This work was supported by the National Natural Science Foundation of China (grant nos. 11675280, 61874139, 11674405 and 61904201) and the Jiangsu Science and Technology Department (Technological Achievements Transformation Project, grant no. BA2017137).

References

Baker-Finch, S.C., McIntosh, K.R., 2011. Reflection of normally incident light from silicon solar cells with pyramidal texture. Prog. Photovolt: Res. Appl. 19, 406–416. https://doi.org/10.1002/pip.1050.

Basher, M.K., Hossain, M.K., Akand, M.A.R., 2019a. Effect of surface texturization on minority carrier lifetime and photovoltaic performance of monocrystalline silicon solar cell. Optik 176, 93–101. https://doi.org/10.1016/j.ijleo.2018.09.042.

Basher, M.K., Hossain, M.K., Uddin, M.J., Akand, M.A.R., Shorowordi, K.M., 2018a. Effect of pyramidal texturization on the optical surface reflectance of monocrystalline photovoltaic silicon wafers. Optik 172, 801–811. https://doi.org/10.1016/j.ijleo.2018.07.116.

Basher, M.K., Khalid Hossain, M., Afaz, R., Tayyaba, S., Akand, M.A.R., Rahman, M.T., Eman, N.M., 2018b. Study and investigation of phosphorus doping time on emitter region for contact resistance optimization of monocrystalline silicon solar cell. Results Phys. 10, 205–211. https://doi.org/10.1016/j.rinp.2018.05.038.

Basher, M.K., Mishan, R., Biswas, S., Khalid Hossain, M., Akand, M.a.R., Matin, M.A., 2019b. Study and analysis the Cu nanoparticle assisted texturization forming low reflective silicon surface for solar cell application. AIP Adv. 9, 075118. https://doi.org/10.1063/1.5109003.

Basher, M.K., Uddin, M.J., Hossain, M.K., Akand, M.A.R., Biswas, S., Mia, M.N.H., Shorowordi, K.M., 2019c. Effect of doping profile on sheet resistance and contact resistance of monocrystalline silicon solar cells. Mater. Res. Express 6, 085510. https://doi.org/10.1088/2053-1591/ab1e8c.

Bidiville, A., Heiber, J., Wasmer, K., Habegger, S., Assi, F., 2010. Diamond wire wafering: wafer morphology in comparison to slurry sawn wafers. Doi: 10.4229/25thEUPVSEC2010-2CV.1.78.

Bidiville, A., Wasmer, K., Kraft, R., Ballif, C., 2009. Diamond wire-sawn silicon wafers - from the lab to the cell production. Proceedings of the 24th EU PV-SEC. https://infoscience.epfl.ch/record/143997 (accessed 2.8.20).

Biegelsen, D.K., Stutzmann, M., 1986. Hyperfine studies of dangling bonds in amorphous

silicon. Phys. Rev. B 33, 3006–3011. https://doi.org/10.1103/PhysRevB.33.3006.
Biswas, S., Basher, M.K., Hossain, M.K., Akand, M.a.R., Rahman, M.T., Ahmed, M.R., Matin, M.A., Huque, S., 2019. Study and analysis of the morphological, elemental and electrical properties of phosphorus doped monocrystalline silicon solar cell. Mater. Res. Express 6, 055515. Doi: 10.1088/2053-1591/ab070b.
Campbell, P., Green, M.A., 1987. Light trapping properties of pyramidally textured surfaces. J. Appl. Phys. 62, 243–249. https://doi.org/10.1063/1.339189.
Cao, Y., Zhou, Yurong, Liu, F., Zhou, Yuqin, Zhang, Y., Liu, Y., Guo, Y., 2015. Progress and mechanism of Cu assisted chemical etching of silicon in a low Cu^{2+} concentration region. ECS J. Solid State Sci. Technol. 4, P331–P336. https://doi.org/10.1149/2.0191508jss.
Chen, K., Liu, Y., Wang, X., Zhang, L., Su, X., 2015. Novel texturing process for diamond-wire-sawn single-crystalline silicon solar cell. Sol. Energy Mater. Sol. Cells 133, 148–155. https://doi.org/10.1016/j.solmat.2014.11.016.
Chen, K., Zha, J., Hu, F., Ye, X., Zou, S., Vähänissi, V., Pearce, J.M., Savin, H., Su, X., 2019. MACE nano-texture process applicable for both single- and multi-crystalline diamond-wire sawn Si solar cells. Sol. Energy Mater. Sol. Cells 191, 1–8. https://doi.org/10.1016/j.solmat.2018.10.015.
Chen, W., Liu, X., Li, M., Yin, C., Zhou, L., 2014. On the nature and removal of saw marks on diamond wire sawn multicrystalline silicon wafers. Mater. Sci. Semicond. Process. 27, 220–227. https://doi.org/10.1016/j.mssp.2014.06.049.
Chen, W., Liu, Y., Yang, L., Wu, J., Chen, Q., Zhao, Y., Wang, Y., Du, X., 2018. Difference in anisotropic etching characteristics of alkaline and copper based acid solutions for single-crystalline Si. Sci. Rep. 8, 3408. https://doi.org/10.1038/s41598-018-21877-x.
Domnich, V., Gogotsi, Y., 2002. Phase transformations in silicon under contact loading. Rev. Adv. Mater. Sci. (Russia) 3, 1–36.
Garnett, E., Yang, P., 2010. Light trapping in silicon nanowire solar cells. Nano Lett. 10, 1082–1087. https://doi.org/10.1021/nl100161z.
Gassilloud, R., Ballif, C., Gasser, P., Buerki, G., Michler, J., 2005. Deformation mechanisms of silicon during nanoscratching: Deformation mechanisms of silicon during nanoscratching. Physica Status Solidi (a) 202, 2858–2869. Doi: 10.1002/pssa.200521259.
Her, T.-H., Finlay, R.J., Wu, C., Deliwala, S., Mazur, E., 1998. Microstructuring of silicon with femtosecond laser pulses. Appl. Phys. Lett. 73, 1673–1675. https://doi.org/10.1063/1.122241.
Hu, J.Z., Merkle, L.D., Menoni, C.S., Spain, I.L., 1986. Crystal data for high-pressure phases of silicon. Phys. Rev. B 34, 4679–4684. https://doi.org/10.1103/PhysRevB.34.4679.
Huang, Z.P., Geyer, N., Liu, L.F., Li, M.Y., Zhong, P., 2010. Metal-assisted electrochemical etching of silicon. Nanotechnology 21, 465301. https://doi.org/10.1088/0957-4484/21/46/465301.
Jenkins, M.W., 1977. A new preferential etch for defects in silicon crystals. J. Electrochem. Soc. 124, 757–762. https://doi.org/10.1149/1.2133401.
Kayes, B.M., Filler, M.A., Putnam, M.C., Kelzenberg, M.D., Lewis, N.S., Atwater, H.A., 2007. Growth of vertically aligned Si wire arrays over large areas (> 1cm2) with Au and Cu catalysts. Appl. Phys. Lett. 91, 103110. https://doi.org/10.1063/1.2779236.
Kelzenberg, M.D., Boettcher, S.W., Petykiewicz, J.A., Turner-Evans, D.B., Putnam, M.C., Warren, E.L., Spurgeon, J.M., Briggs, R.M., Lewis, N.S., Atwater, H.A., 2010. Enhanced absorption and carrier collection in Si wire arrays for photovoltaic applications. Nat. Mater 9, 239–244. https://doi.org/10.1038/nmat2635.
Kulkarni, M.S., Libbert, J., Keltner, S., Muléstagno, L., 2002. A theoretical and experimental analysis of macrodecoration of defects in monocrystalline silicon. J. Electrochem. Soc. 149, G153. https://doi.org/10.1149/1.1433473.
Lee, J.-P., Choi, S., Park, S., 2011. Extremely superhydrophobic surfaces with micro- and nanostructures fabricated by copper catalytic etching. Langmuir 27, 809–814. https://doi.org/10.1021/la1045354.
Li, J.-Y., Hung, C.-H., Chen, C.-Y., 2017. Hybrid black silicon solar cells textured with the interplay of copper-induced galvanic displacement. Sci. Rep. 7. https://doi.org/10.1038/s41598-017-17516-6.
Lippold, M., Buchholz, F., Gondek, C., Honeit, F., Wefringhaus, E., Kroke, E., 2014. Texturing of SiC-slurry and diamond wire sawn silicon wafers by HF–HNO3–H2SO4 mixtures. Sol. Energy Mater. Sol. Cells 127, 104–110. https://doi.org/10.1016/j.solmat.2014.04.006.
Lu, Y.-T., Barron, A.R., 2014. Anti-reflection layers fabricated by a one-step copper-assisted chemical etching with inverted pyramidal structures intermediate between texturing and nanopore-type black silicon. J. Mater. Chem. A 2, 12043. https://doi.org/10.1039/C4TA02006E.
Meinel, B., Koschwitz, T., Acker, J., 2012. Textural development of SiC and diamond wire sawed sc-silicon wafer. Energy Procedia 27, 330–336. https://doi.org/10.1016/j.egypro.2012.07.072.
Nayak, B.K., Iyengar, V.V., Gupta, M.C., 2011. Efficient light trapping in silicon solar cells by ultrafast-laser-induced self-assembled micro/nano structures. Prog. Photovoltaics Res. Appl. 19, 631–639. https://doi.org/10.1002/pip.1067.
Sai, H., Fujii, H., Arafune, K., Ohshita, Y., Yamaguchi, M., Kanamori, Y., Yugami, H., 2006. Antireflective subwavelength structures on crystalline Si fabricated using directly formed anodic porous alumina masks. Appl. Phys. Lett. 88, 201116. https://doi.org/10.1063/1.2205173.
Vazsonyi, E., De Clercq, K., Einhaus, R., Van Kerschaver, E., Said, K., Poortmans, J., Szlufcik, J., Nijs, J., 1999. Improved anisotropic etching process for industrial texturing of silicon solar cells. Sol. Energy Mater. Sol. Cells 57, 179–188. https://doi.org/10.1016/S0927-0248(98)00180-9.
Wang, Y., Liu, Y., Yang, L., Chen, W., Du, X., Kuznetsov, A., 2017. Micro-structured inverted pyramid texturization of Si inspired by self-assembled Cu nanoparticles. Nanoscale 9, 907–914. https://doi.org/10.1039/C6NR08126F.
Wang, Y., Yang, L., Liu, Y., Mei, Z., Chen, W., Li, J., Liang, H., Kuznetsov, A., Xiaolong, D., 2015. Maskless inverted pyramid texturization of silicon. Sci. Rep. 5, 10843. https://doi.org/10.1038/srep10843.
Wu, J., Liu, Y., Chen, Q., Chen, W., Yang, L., Wang, Y., He, M., Du, X., 2018. The orientation and optical properties of inverted-pyramid-like structures on multi-crystalline silicon textured by Cu-assisted chemical etching. Sol. Energy 171, 675–680. https://doi.org/10.1016/j.solener.2018.07.011.
Yang, L., Liu, Y., Wang, Y., Chen, W., Chen, Q., Wu, J., Kuznetsov, A., Du, X., 2017. 18.87%-efficient inverted pyramid structured silicon solar cell by one-step Cu-assisted texturization technique. Sol. Energy Mater. Sol. Cells 166, 121–126. https://doi.org/10.1016/j.solmat.2017.03.017.
Yang, X., Zhang, W., Choi, J., Ta, H.Q., Bai, Y., Chen, L., Zhang, M., Chen, Y., Guan, Z., Rummeli, M.H., Liu, L., 2019. Influence of bowl-like nanostructures on the efficiency and module power of black silicon solar cells. Sol. Energy 189, 67–73. https://doi.org/10.1016/j.solener.2019.07.044.
Zhao, S., Yuan, G., Wang, Q., Liu, W., Zhang, S., Liu, Z., Wang, J., Li, J., 2019a. Morphology control of c-Si via facile copper-assisted chemical etching: Managements on etch end-points. Appl. Surf. Sci. 489, 776–785. https://doi.org/10.1016/j.apsusc.2019.06.032.
Zhao, Y., Liu, Y., Chen, Q., Chen, W., Wu, J., Wang, Y., Du, X., 2019b. Broadband omnidirectional anti-reflection property of V-groove textured silicon. Sol. Energy 193, 132–138. https://doi.org/10.1016/j.solener.2019.09.048.
Zheng, H., Han, M., Zheng, P., Zheng, L., Qin, H., Deng, L., 2014. Porous silicon templates prepared by Cu-assisted chemical etching. Mater. Lett. 118, 146–149. https://doi.org/10.1016/j.matlet.2013.12.093.
Zhuang, Y.F., Zhong, S.H., Huang, Z.G., Shen, W.Z., 2016. Versatile strategies for improving the performance of diamond wire sawn mc-Si solar cells. Sol. Energy Mater. Sol. Cells 153, 18–24. https://doi.org/10.1016/j.solmat.2016.04.014.